Available online at www.sciencedirect.com
SCIENCE DIRECT
Lithos 90 (2006) 92–110
LITHOS
www.elsevier.com/locate/lithos

Interaction between basic and acid magmas during the latest stages of the post-collisional Variscan evolution: Clues from the gabbro–granite association of Ota (Corsica–Sardinia batholith)

Maria Rosaria Renna [a,*], Riccardo Tribuzio [a,b], Massimo Tiepolo [b]

[a] *Dipartimento di Scienze della Terra, Università di Pavia, Via Ferrata 1, 27100 Pavia, Italy*
[b] *C.N.R.—Istituto di Geoscienze e Georisorse, Unità di Pavia, Via Ferrata 1, 27100 Pavia, Italy*

Received 10 November 2004; accepted 10 February 2006
Available online 31 March 2006

Abstract

The intrusive association of Ota (post-Variscan Corsica–Sardinia batholith) consists of mafic rocks and granites displaying mingling relations. The mafic rocks are olivine gabbros to quartz-diorites, and the granites are subsolvus and characterised by biotite as the only mafic phase. Minor amounts of amphibole-bearing granodiorites to granites develop along the contacts between mafic rocks and granites. The rather high initial ε_{Nd} (+4.5) of the most primitive mafic sample indicates that parental basic melts had an extensive contribution from a depleted mantle source. In the mafic rocks, the decrease of initial ε_{Nd} (to +2.1) is associated with an increase of Th and U concentrations in clinopyroxene, thus indicating that the Ota basic melts underwent a process of crustal contamination. Associated biotite granites have low initial ε_{Nd} (+0.4) and high Th and U concentrations. The chemical evolution of Ota basic melts most likely occurred through fractional crystallisation and concomitant contamination with the acid magma that gave rise to associated biotite granites. The incompatible element signature of late-stage anhedral amphibole from variably evolved mafic rocks is similar, thus suggesting that the whole Ota mafic sequence recorded the contamination process, possibly by percolation within the gabbroic crystal mush of a melt contaminated by the acid magma. Hybridisation between basic and acid magmas is also documented by contact amphibole-bearing granitoids. In particular, major and trace element zoning of amphibole from granodiorites reveals that such a hybridisation was associated with reactions between crystals from the basic magma (amphibole and clinopyroxene) and the acid melt. The occurrence of chemically homogeneous amphiboles in associated granites suggests that "contact" hybridisation comprised also a process of gradient-induced chemical diffusion.

1. Introduction

The understanding of the mechanisms controlling the interaction of basic and acid magmas in plutonic contexts has benefited from many studies of the post-Variscan Corsica–Sardinia batholith (e.g. Orsini et al., 1991; Poli et al., 1996). One of the most spectacular field-scale terrains showing basic–acid magma interaction in the Corsica–Sardinia batholith is represented by the gabbro–granite association of Ota (western Corsica), which was related to the latest "anorogenic" stage of the Variscan cycle (Bonin, 1988; Bonin et al., 1998). Mingling textures at the field scale were attributed to limited hybridisation between basic and acid magmas

* Corresponding author. Tel.: +39 0382 985839; fax: +39 0382 985890.
E-mail address: renna@crystal.unipv.it (M.R. Renna).

0024-4937/$ - see front matter © 2006 Elsevier B.V. All rights reserved.
doi:10.1016/j.lithos.2006.02.003

(Platevoet and Bonin, 1991), and the granite sources were ascribed to lower crustal reservoirs (Poitrasson et al., 1995), but little is known about the igneous evolution of mafic and hybrid rocks.

This paper aims to decipher the processes related to the interaction of basic and acid magmas in plutonic post-collisional settings. For this purpose, we have carried out a study of the gabbro–granite association of Ota, by coupling field and petrographic investigations with major, trace element and Nd isotope analyses of whole-rocks. In addition, we have also considered the trace element compositions of clinopyroxene and amphibole, determined by laser ablation ICP-MS. Remarkably, trace element mineral compositions have been only rarely utilised to unravel the origin of hybrid plutonics, although they yielded valuable geochemical information to the petrogenetic comprehension of intrusive rocks with disequilibrium textures (e.g. Blundy and Shimizu, 1991). The adopted methodological approach has allowed us to give new insights into the processes related to the interaction between basic and acid magmas in the Ota association. In addition, new information about the composition of mantle-derived melts involved in the development of the Corsica batholith during the post-collisional phase of the Variscan orogeny have been provided.

1.1. Geological setting

The Corsica–Sardinia batholith developed during the post-collisional phase of the Variscan orogeny and consists mostly of Middle Carboniferous to Permian granitoids. Three main plutonic suites are recognised in the Corsican sector of the batholith (Fig. 1a). The oldest intrusions (340–320 Ma) consist mainly of Mg- and K-rich granitoids with shoshonitic affinity (Cocherie et al., 1994; Ferré and Leake, 2001; Paquette et al., 2003). The subsequent intrusions are about 305 Ma old and volumetrically dominated by low-K hornblende granitoids defining calc-alkaline trends (Cocherie et al., 1994; Tommasini et al., 1995; Paquette et al., 2003). These plutonic suites were locally intruded by gabbroic sequences whose geochemical affinity is still debated (cf. Cocherie et al., 1994; Tommasini et al., 1995; Bonin, 2004), and by peralkaline to slightly peraluminous A-type granites (Bonin et al., 1978; Egeberg et al.,

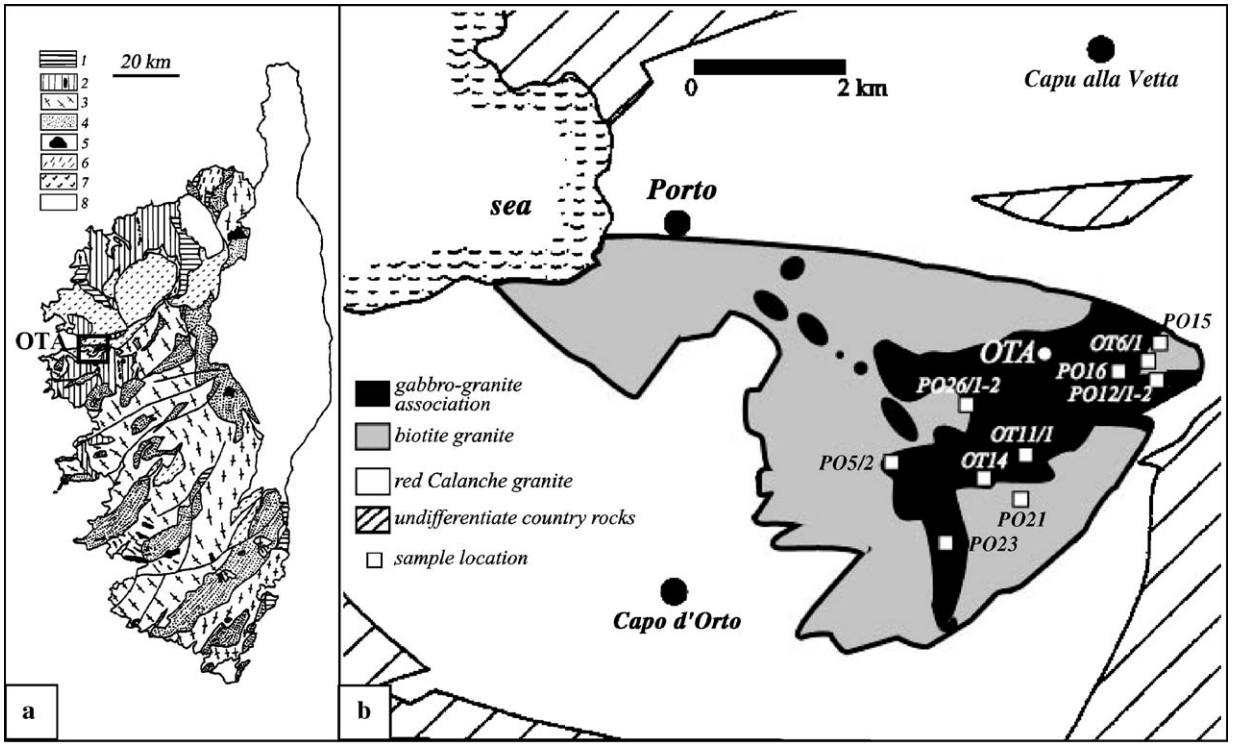

Fig. 1. (a) Schematic geologic map of Corsica Island (slightly modified after Cocherie et al., 1994). 1=metamorphic basement; 2=Mg–K granitoids (vertical stripes) and included biotite-rich rocks (black patches); 3=calk-alkaline granodiorites to monzogranites; 4=calk-alkaline leucomonzogranites; 5=gabbroic sequences; 6=calk-alkaline volcanic rocks; 7=alkaline intrusive and volcanic rocks; 8=post-batholithic formations. (b) Schematic geologic map of the Porto Complex (slightly modified after Vellutini, 1975) and location of selected samples.

1993; Poitrasson et al., 1994, 1995). Recent geochronological determinations based on zircon investigations have provided intrusion ages of 280–290 Ma for both gabbroic sequences and A-type granites (Paquette et al., 2003; Cocherie et al., 2005).

The Porto complex from western Corsica consists (Fig. 1b) of a central gabbro–granite association (known as Ota association) displaying mingling relations, and a marginal red Calanche granite that was interpreted as a later ring-dyke (Vellutini, 1975; Bonin, 1988; Platevoet et al., 1988; Platevoet and Bonin, 1991). The Ota mafic rocks were dated through K–Ar determinations on hornblende and biotite at 282±10 Ma (Edel et al., 1981). Consistently, the associated granites gave K–Ar biotite ages of 276±4 Ma and 285±5 Ma, and a Rb–Sr whole rock-biotite isochron of 287±6 Ma (van Tellingen et al., 1996). Previous petrological and geochemical studies of the Ota association were mainly devoted to the origin of the granites (Poitrasson et al., 1995), which are subsolvus and characterised by biotite as the only mafic phase. According to Poitrasson et al. (1995), the Ota biotite granites show distinctive geochemical features of A-type granites and their parental liquids were most likely derived from partial melting of lower crustal mafic rocks.

1.2. Field relations

The mafic rocks form bodies (up to tens of metres in size) enclosed into biotite granites. Along the contacts between the largest mafic rock bodies and granites, round to slightly flattened pillow-like mafic blobs commonly occur (Fig. 2a). These pillow-like bodies reach up to a couple of metres in size and generally display grain-size decrease against the host granitoids. Granite dykelets displaying irregular contacts towards the host mafic rock are locally found within both pillow-like mafic blobs and large mafic rock bodies. Thin K-feldspar-rich veins are also found within the large mafic rock bodies near the contact with the granitoids, and are closely associated with large K-feldspar grains that are commonly elongated along the same direction of the vein (Fig. 2b). These veins indicate that residual acid melts migrated from the contact zone towards the mafic bodies. Fine-grained K-feldspar-rich veins with sharp contacts, most likely related to back-veining phenomena, are also present.

Close to the pillow-like mafic blobs, for lengths that commonly do not exceed a few tens of centimetres, the granitoids are characterised by the presence of amphibole (see also Platevoet and Bonin, 1991). The amphibole-bearing granitoids are texturally heterogeneous. The textural heterogeneity is mainly given by the random arrangement of cm-scale mafic enclaves

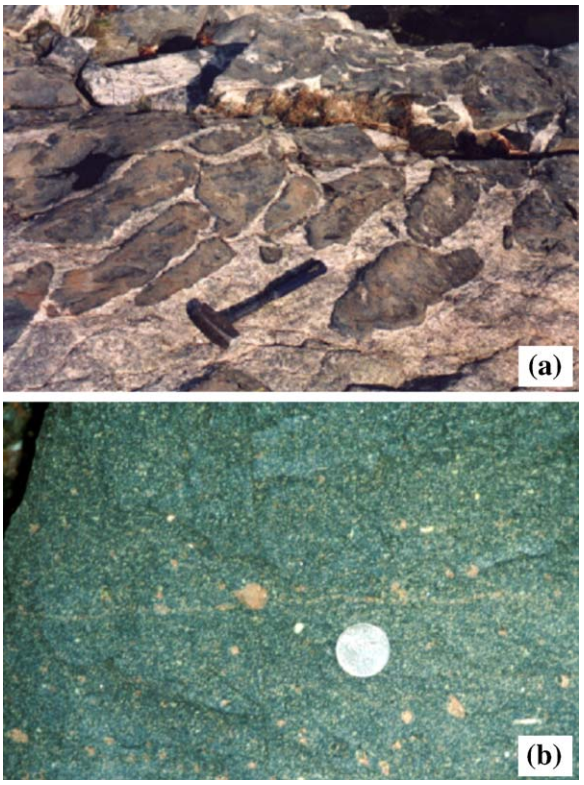

Fig. 2. Photographs showing main field relations of the mafic and granitoid rocks in the Ota association. (a) Pillow-like blobs developed along a contact between a large mafic rock body and enclosing biotite granites. The granitoids associated with the mafic blobs are amphibole-bearing and contain glomeroporphyritic clots rich in amphibole. (b) Thin K-feldspar-rich veins within the large mafic rock bodies, closely associated with large K-feldspar grains that are commonly elongated along the same direction of the vein.

displaying irregular shape, glomeroporphyritic clots rich in amphibole and biotite (up to a couple of cm in size), and mm-scale quartz ocelli rimmed by amphibole. In addition, the amphibole-bearing granitoids contain in places coarse-grained dykelets rich in K-feldspar, which display irregular contacts towards the host rock. The occurrence of such dykelets suggests that the mingling between the two magmas with contrasting compositions was associated with a process of mineral fractionation and accumulation that led to the development of K-rich residual melts. Locally, the amphibole-bearing granitoids constitute metre-scale bodies including disseminated centimetre-scale mafic blobs with round shape.

1.3. Analytical techniques

Field and petrographic investigations allowed us to select a group of 12 representative rock samples which were classified on the basis of their modal compositions.

They include 5 mafic rocks, 5 amphibole-bearing granitoids and two amphibole-free biotite granites.

Whole-rock chemical compositions (Table 4) of eight samples were attained at the European Union Large Scale Geochemical Facility (Department of Earth Sciences, University of Bristol). Major and trace (Ba, Co, Cu, Ga, Hf, P, Pb, Rb, Sn, Sr, V, Y, Zn, Zr) elements were determined by conventional X-ray fluorescence (XRF) techniques, and the concentrations of rare earth elements (REE), U, Th, Nb, Ta were determined by inductively coupled plasma mass spectrometry (ICP-MS). Whole-rock major and trace element compositions of three samples were obtained by ICP-MS at Activation Laboratories (Ancaster, Ontario). Cr and Ni concentrations were determined only for the mafic rocks, by XRF at Dipartimento di Scienze della Terra, Università di Parma. Precision and accuracy of XRF analyses are within 5% for Cr, Ni, Cu, Zn, Ga, Rb, Sr, Ba, Zr and Y, and within 20% for V, Co, Sn and Pb. Hf analyses by XRF are affected by a large uncertainty (<50%) as the measured concentrations are close to the detection limit. Precision and accuracy of ICP-MS analyses are commonly within 10%.

Nd isotope composition of samples PO5-2, PO16, PO12-1, PO26-2, PO26-1 and OT6-1 (Table 5) were determined at Activation Laboratories (Ancaster, Ontario). Samples were dissolved in a mixture of Hf, HNO_3 and $HClO_4$. The analyses were performed on Finnigan MAT 261 8-collector mass-spectrometer in static mode. $^{143}Nd/^{144}Nd$ ratios are relative to the value of 0.511860 for the La Jolla standard. During the period of work the weighted average of 10 La Jolla Nd-standard runs yielded 0.511852±5 (2 S.E.) for $^{143}Nd/^{144}Nd$. Data are corrected for $^{143}Nd/^{144}Nd=0.511860$.

Electron microprobe analyses of plagioclase, amphibole, olivine and clinopyroxene were carried out at C.N.R.—Istituto di Geoscienze e Georisorse, Unità di Firenze, with a JEOL JXA-8600 equipped with four wavelength dispersive spectrometers and an energy dispersive spectrometer. Operating conditions were 15 kV accelerating voltage, 10 nA beam current, 10 s counting time for Na and 15 s for the other major elements (Vaggelli et al., 1999).

Trace element compositions of clinopyroxene and amphibole were determined by laser ablation inductively coupled plasma-mass spectrometry at C.N.R.—Istituto di Geoscienze e Georisorse, Unità di Pavia. The instrument couples a pulsed Nd:YAG laser source "Brilliant" (Quantel, Les Ulis, France) working at 213 nm with a sector field ICP mass spectrometer "Element I" from ThermoFinnigan. The reader is referred to Tiepolo et al. (2003) for details about the analytical method. For the present study the laser was operated at a repetition rate of 10 Hz, and the spot diameter was ~45 μm with a pulse energy of about 0.15 mJ. Ablation signal and integration intervals were selected by carefully inspecting the time-resolved analysis to ensure that no inclusions were present in the analysed volume, and data reduction was performed by the software package "Glitter" (van Achterbergh et al., 1999). NIST SRM 612 and ^{44}Ca were used as external and internal standards, respectively. Reproducibility and accuracy of concentration values were assessed on the control sample BCR2-g (MUN, ICP-MS unpublished data) to be <7% and <10%, respectively.

Table 1
Visually estimated modal compositions of selected samples

Sample	PO5-2	PO16	OT14	PO12-1	PO23	PO26-2	OT11-1	PO21	PO12-2	PO26-1	OT6-1	PO15
Rock-type	Ol-G	Cpx-G	Qtz-D	Qtz-D	Qtz-D	Gr	Gr	Amp-G	Amp-G	Amp-G	Bt-G	Bt-G
Modal composition (vol.%)												
Ol	tr	–	–	–	–	–	–	–	–	–	–	–
Cpx	20	20	5	5	tr	–	–	–	–	–	–	–
Pl	50	50	50	45	45	30	30	25	20	30	25	25
Amp	30	30	35	25	25	25	30	15	15	5	–	–
Bt	–	–	5	15	15	20	20	10	10	10	5	10
Qtz	–	–	5	10	10	15	15	30	30	30	35	35
Kfs	–	–	tr	tr	5	10	5	20	25	25	35	30
Ap	tr	tr	tr	tr	tr	tr	tr	tr	tr	tr	tr	tr
Ilm/Mag	tr	tr	tr	tr	tr	tr	tr	tr	tr	tr	tr	tr
Zrn	–	–	tr	tr	tr	tr	tr	tr	tr	tr	tr	tr
Aln	–	–	–	–	–	–	–	tr	tr	tr	tr	tr
Pl alteration	+	+	+	++	++	+	++	+	++	+	+	+
Bt chloritisation	++	++	++	++	++	++	++	+	+	+	+	+

Mineral abbreviations according to Kretz (1983); tr, trace amount; –, mineral not present in the rock.
Extent of Pl alteration and Bt chloritisation: +, 20–60%; ++, >60%. Ol-G, olivine-bearing gabbro; Cpx-G, olivine-free gabbro; Qtz-D, quartz-diorite; Gr, granodiorite; Amp-G, amphibole-bearing granite; Bt-G, biotite-bearing granite.

2. Main petrological features of selected samples

2.1. Mafic rocks

Two gabbros, which occur only in the largest mafic rock bodies, and three quartz-diorites have been selected (Table 1). The gabbros are medium-grained and mainly constituted by plagioclase, clinopyroxene and amphibole. Plagioclase crystals are slightly zoned, with a compositional range from An_{65} to An_{60} at the cores and from An_{58} to An_{34} at the rims (Renna, 2004). Clinopyroxene is ophitic and is commonly rimmed by red–brown amphibole (Fig. 3a). The latter also occurs as large anhedral grains that locally include ilmenite. According to the classification of Leake et al. (1997), they are edenites. In the gabbro PO16, amphibole is locally optically zoned showing red–brown core and green rim. One of the two samples contains minor

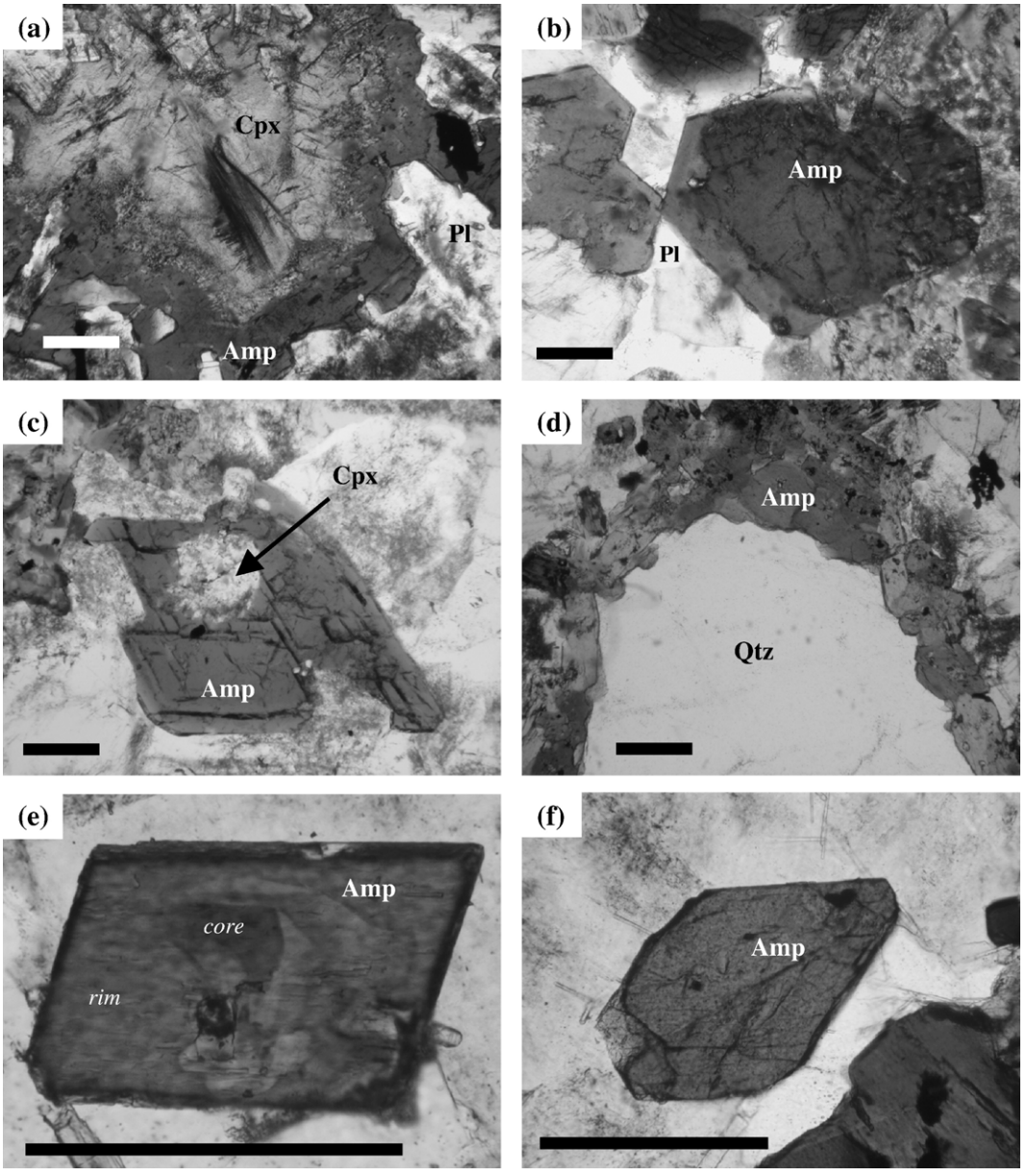

Fig. 3. Thin section photomicrographs (scale bar = 0.25 mm; mineral abbreviations are after Kretz, 1983). (a) Ophitic clinopyroxene rimmed by red–brown amphibole in olivine-free gabbro; (b) amphibole grain from quartz-diorite displaying red–brown core and green rim; (c) relic of clinopyroxene within amphibole core from quartz-diorite; (d) quartz *ocellus* rimmed by amphibole from granodiorite; (e) zoned amphibole from granodiorite, with brownish core and green rim; (f) optically homogeneous amphibole grain from granite.

Table 2
Representative electron microprobe analyses of olivine and clinopyroxene

Sample	PO5/2	PO18-1	PO12/1	PO12/1
Rock-type	Ol-G	Cpx-G	Qtz-D	Qtz-D
wt.%	Cpx	Cpx	Cpx	Cpx
SiO_2	36.9	48.9	49.5	50.0
TiO_2	0.04	2.06	1.72	1.28
Al_2O_3	0.08	5.29	4.11	3.79
Cr_2O_3	<0.01	0.25	0.06	0.02
FeO	33.4	8.18	9.79	10.5
MnO	0.67	0.23	0.27	0.38
MgO	30.6	13.5	13.9	12.8
CaO	0.09	20.8	20.2	20.0
Na_2O	0.00	0.48	0.60	0.78
NiO	0.07	/	/	/
Sum	101.7	99.7	100.1	99.5
Mg#	0.62	0.75	0.72	0.68

Ol-G, olivine-bearing gabbro; Cpx-G, olivine-free gabbro; Qtz-D, Quartz-diorite. /: not analysed.
$Mg\# = Mg^{2+}/(Mg^{2+}+Fe^{2+}+Fe^{3+})$.
Fe^{3+} was calculated assuming stoichiometry.

amounts of olivine (Fo = 62 mol%, Table 2). Apatite, zircon and biotite occur as scarce accessory phases.

The quartz-diorites are medium- to fine-grained and show hypidiomorphic texture. They mainly consist of plagioclase, amphibole, and biotite with variable modal proportions. Minor amounts of quartz and perthitic alkali feldspar are locally present; ilmenite, apatite and zircon are common accessory phases. Ilmenite is generally skeletal and apatite has acicular habit, most likely as a result of the rapid cooling of the basic melt in response to the interaction with the acid magma (see also Wyllie et al., 1962; Hibbard, 1991; Vernon, 1991). In quartz-diorite plagioclase is relatively poorer in anorthite component (An_{31-18}) than gabbros, but locally anorthite-rich cores (up to 49 mol%) were found (Renna, 2004). Clinopyroxene is locally found as relics, particularly within amphibole cores (Fig. 3c); it exhibits lower Al_2O_3, TiO_2, MgO and higher MnO contents than that from the gabbros (Table 2). Amphibole shows subhedral habit. Red–brown cores and oscillatory zoned greenish to green rims are commonly recognisable (Fig. 3b), but in a few samples (e.g. PO12/1), the red–brown cores are not preserved. Greenish to green amphibole rims are mainly Mg-hornblendes and display lower Al_2O_3, Na_2O and TiO_2 than the edenitic red–brown cores (Table 3).

2.2. Granitoids

Five samples of amphibole-bearing granitoids have been selected. They mainly consist of plagioclase, amphibole, biotite, perthitic K-feldspar and quartz. Acicular apatite, skeletal Fe–Ti-oxide phases, and zircon are frequent accessory phases. On the basis of estimated modal amounts (Table 1), they are classified as granodiorites to granites. Both rock-types have large quartz crystals (ocelli, up to 6 mm in size) mantled by amphibole (Fig. 3d), which are less abundant and smaller in the granites than in granodiorites. Plagioclase is relatively poor in anorthitic component, which ranges from An_{24} to An_{15} (Renna, 2004). Amphibole from the granodiorites is commonly optically zoned, with brownish cores and green rims (Fig. 3e). The brownish cores have higher Al_2O_3, Na_2O and TiO_2 than the green rims (edenites and Mg-hornblendes, respectively) and chemically approach the red–brown amphiboles from

Table 3
Representative electron microprobe analyses of amphiboles

Sample	PO5/2	PO23	PO23	PO12/1	PO26/2	PO26/2	PO21	PO26/1
Rock-type	Ol-G	Qtz-D	Qtz-D	Qtz-D	Gr	Gr	Amp-G	Amp-G
Amp wt.%	Red–brown core	Red–brown core	Greenish to green rim	Greenish to green rim	Brownish core	Green rim	Core	Core
SiO_2	44.69	43.44	48.42	47.57	44.91	47.79	46.57	47.22
TiO_2	2.66	3.67	1.30	1.27	2.33	1.61	1.41	1.36
Al_2O_3	8.75	9.69	5.12	5.86	7.86	6.27	6.09	5.62
FeO	14.33	15.75	16.09	18.13	17.60	16.64	19.42	18.94
MnO	0.25	0.09	0.19	0.37	0.32	0.33	0.42	0.42
MgO	13.93	11.46	13.14	11.51	11.22	12.10	10.97	11.28
CaO	9.94	10.60	10.77	10.53	10.29	10.53	10.42	10.06
Na_2O	2.42	2.07	1.18	1.21	1.79	1.49	1.70	1.73
K_2O	0.56	0.78	0.42	0.53	0.80	0.56	0.67	0.64
Sum	97.53	97.55	96.63	96.98	97.12	97.32	97.67	97.27
Mg#	0.63	0.56	0.59	0.53	0.53	0.56	0.50	0.51

Ol-G, olivine-bearing gabbro; Cpx-G, olivine-free gabbro; Qtz-D, quartz-diorite; Gr, granodiorite; Amp-G, amphibole-bearing granite.
$Mg\# = Mg^{2+}/(Mg^{2+}+Fe^{2+})$, assuming $Fe^{3+}=0$. Cr_2O_3 below detection limit.

mafic rocks (Table 3). On the other hand, amphibole from the granites is homogeneously green (Fig. 3f) and plot within both edenite and Mg-hornblende classification fields of Leake et al. (1997). The granites are characterised by the local occurrence of accessory allanite and granophyric textures.

Two samples of amphibole-free biotite granites have been selected. They are medium- to coarse-grained and nearly equigranular. They consist of perthitic K-feldspar, quartz, plagioclase and minor biotite. The latter mostly occurs as inclusion in quartz and K-feldspar. Common accessory phases are zircon, allanite, Fe–Ti oxide phases and acicular apatite. Anorthite contents in plagioclase range from An_{17} to An_{10} (Renna, 2004). Granophyric and myrmekitic textures are present locally.

3. Whole-rock geochemistry

3.1. Mafic rocks

The gabbros have higher Mg# ($MgO/MgO+FeO^{tot}$) and Al_2O_3, and lower TiO_2, K_2O, P_2O_5 and MnO than quartz-diorites (Fig. 4, Table 4). In particular, the olivine gabbro shows the highest Mg#, Al_2O_3 and CaO, and the lowest K_2O values. The concentrations of Ni and Cr are overall relatively low (52–136 ppm and 130–276 ppm), with the highest values pertaining to the olivine gabbro.

The concentrations of incompatible trace elements, with the exception of Sr, increase from the olivine gabbro to olivine-free gabbro and quartz-diorites (Fig. 5). The N-MORB normalised patterns of REE and HFSE are nearly parallel. Remarkably, Nb is slightly enriched and slightly depleted relative to La in gabbros and quartz-diorites, respectively. The pattern of olivine gabbro is characterised by Sr enrichment relative to LREE and weak positive Eu anomaly ($Eu/Eu^*=1.1$), thus suggesting that this rock records a process of plagioclase accumulation. On the other hand, the quartz-diorites display a negative Sr anomaly. Large variations have been observed for Rb, Th, U and Pb, with the lowest and the highest abundances pertaining to the olivine gabbro and the quartz-diorite PO12/1, respectively.

The olivine gabbro shows the highest initial ε_{Nd} value (+4.5, Fig. 6), which decreases at +2.4 and +2.1 for the olivine-free gabbro and quartz-diorite PO12-1, respectively. The Nd isotope compositions of selected samples are slightly depleted relative to those reported by Poitrasson et al. (1995) for the Ota mafic rocks, which have $\varepsilon_{Nd(280\,Ma)}$ ranging from +2.0 to +0.8. Remarkably, samples PO5-2 (this study) and 85048

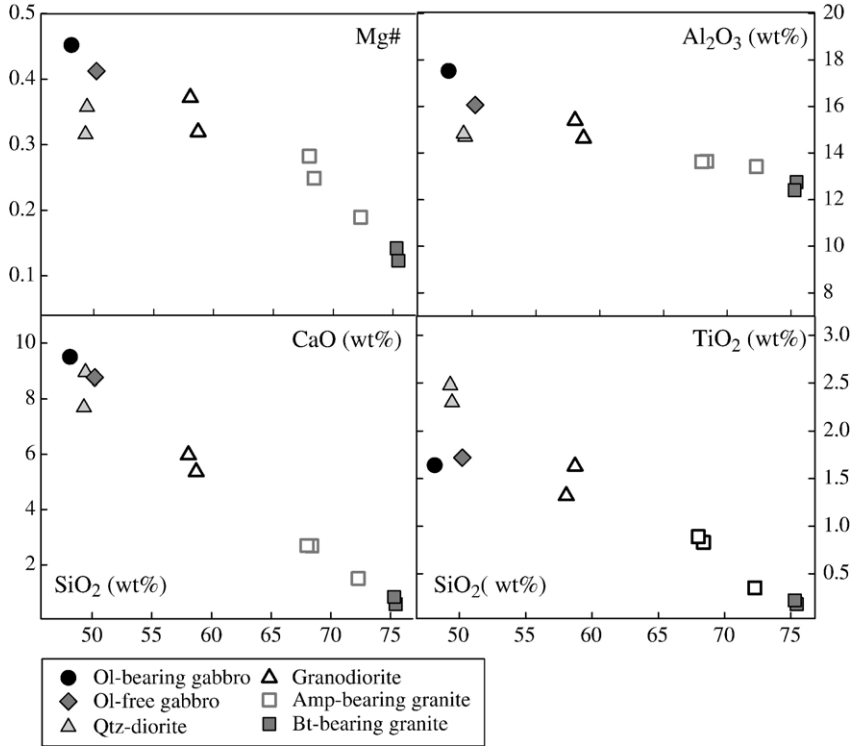

Fig. 4. Major element whole-rock variations: Mg# ($MgO/MgO+FeO^{tot}$), Al_2O_3, CaO and TiO_2 vs. SiO_2.

Table 4
Whole-rock major and trace element compositions of selected samples

Sample	PO5/2 [a]	PO16	PO12/1	PO26/2	OT11/1 [a]	PO21	PO12/2 [a]	PO26-1	OT6/1	PO15	PO15
Rock-type	Ol-G	Cpx-G	Qtz-D	Gr	Gr	Amp-G	Amp-G	Amp-G	Bt-G	Bt-G	Bt-G
Major elements (wt.%)											
SiO_2	48.13	50.22	49.44	49.31	58.06	58.72	68.40	68.01	72.29	75.44	75.29
TiO_2	1.64	1.72	2.30	2.48	1.32	1.63	0.83	0.89	0.35	0.18	0.22
Al_2O_3	17.53	16.07	14.70	14.83	15.40	14.64	13.65	13.63	13.42	12.76	12.41
$Fe_2O_3^{tot}$	10.10	10.41	11.69	12.55	7.38	8.14	4.38	4.71	2.68	1.52	1.80
MnO	0.16	0.16	0.19	0.20	0.11	0.13	0.07	0.08	0.03	0.02	0.02
MgO	7.50	6.58	5.86	5.21	3.93	3.44	1.31	1.67	0.56	0.19	0.27
CaO	9.50	8.76	8.95	7.69	5.97	5.36	2.69	2.70	1.51	0.58	0.84
Na_2O	3.43	3.46	3.42	3.52	4.20	3.98	4.42	3.85	3.50	3.52	3.46
K_2O	0.52	0.89	1.21	1.93	2.33	2.19	3.41	3.49	4.90	5.33	4.97
P_2O_5	0.28	0.30	0.61	0.53	0.26	0.44	0.19	0.20	0.09	0.04	0.06
L.O.I	1.52	1.01	1.16	1.23	0.74	1.43	0.46	0.88	0.42	0.25	0.45
Sum	100.30	99.57	99.53	99.48	99.71	100.10	99.79	100.11	99.75	99.83	99.78
Mg#	0.45	0.41	0.36	0.32	0.37	0.32	0.25	0.28	0.19	0.12	0.14
Trace elements (ppm)											
V	192	174	234	252	142	161	53	83.7	22	<6	12
Cr	276	188	213	130	n.a.	n.a.	n.a.	n.a.	n.a.	n.a.	n.a.
Co	42.1	49	43	47	34	20.0	20	10.5	12	<10	10
Ni	136	63	71	52	n.a.	n.a.	n.a.	n.a.	n.a.	n.a.	n.a.
Cu	46.0	36.7	20.7	26.1	20.7	18.8	3.4	<10	<0.5	<0.5	<0.5
Zn	73.8	78.7	93.5	121	65.2	94.2	50.4	82.1	22.3	21.2	17.8
Ga	18.9	19.1	19.7	21.4	19.3	22.3	20.1	21.9	17.9	18.6	17.9
Sn	1.3	2	2	2	4	5.9	5	6.0	6	4	2
Rb	15.6	25.9	32.3	78.1	92.4	91.2	132	133	157	163	128
Sr	370	312	316	265	228	253	114	149	96.8	52.1	77.4
Ba	134	173	321	324	211	323	179	272	225	242	291
Zr	147	154	225	249	165	272	114	196	134	122	174
Nb	11.7	14.5	19.2	16.5	18.6	19.3	26.4	20.4	27.6	23.8	20.9
Y	28.3	28.6	41.9	44.1	34.3	44.2	43.8	43.6	31.1	32.8	24.6
Hf	3.4	3	6	8	5	6.7	5	5.9	7	5	7
Ta	0.50	1.32	1.08	1.02	1.17	1.22	1.73	1.44	1.31	1.61	0.92
Pb	<5	6	7	12	12	9.1	17	11.0	20	25	22
Th	1.09	3.19	2.91	7.09	10.5	10.4	18.5	19.3	23.4	22.9	20.6
U	0.36	0.71	0.58	1.68	2.95	3.71	5.15	5.83	5.24	3.76	2.48
La	11.5	17.8	28.9	27.0	26.2	33.3	49.7	56.3	31.8	56.2	74.3
Ce	27.1	40.0	67.6	61.8	56.4	68.7	103	103	63.9	111	143
Pr	3.86	5.36	9.21	8.33	6.99	8.84	11.8	11.6	7.29	12.0	14.5
Nd	16.3	22.7	39.9	35.5	27.7	33.2	42.6	37.5	25.5	39.0	46.2
Sm	4.52	5.46	9.43	8.49	6.37	7.95	8.89	7.98	5.29	6.90	7.30
Eu	1.73	1.73	2.89	2.59	1.46	2.04	1.00	1.14	0.65	0.46	0.57
Gd	4.71	5.63	9.35	8.52	6.39	7.65	8.19	7.18	5.02	5.65	5.76
Tb	0.83	0.88	1.45	1.33	1.01	1.29	1.34	1.22	0.80	0.88	0.77
Dy	4.93	5.31	8.36	7.93	6.17	7.52	7.86	7.03	4.89	5.12	4.31
Ho	1.00	1.06	1.70	1.60	1.24	1.54	1.59	1.44	1.02	0.99	0.78
Er	2.84	2.94	4.65	4.44	3.51	4.41	4.68	4.27	2.96	2.92	2.16
Tm	0.41	0.42	0.64	0.64	0.50	0.65	0.70	0.65	0.45	0.45	0.31
Yb	2.51	2.60	3.95	3.88	3.21	4.06	4.18	3.97	2.88	2.91	1.99
Lu	0.40	0.36	0.57	0.55	0.45	0.64	0.58	0.62	0.40	0.40	0.27

Ol-G, olivine-bearing gabbro; Cpx-G, olivine-free gabbro; Qtz-D, quartz-diorite; Gr, granodiorite; Amp-G, amphibole-bearing granite; Bt-G, biotite-bearing granite.

L.O.I.: loss on ignition. Mg# = MgO/(MgO + FeO^{tot}). n.a. = not analysed.

[a] Whole-rock compositions determined at the Activation Laboratories (Ancaster, Ontario).

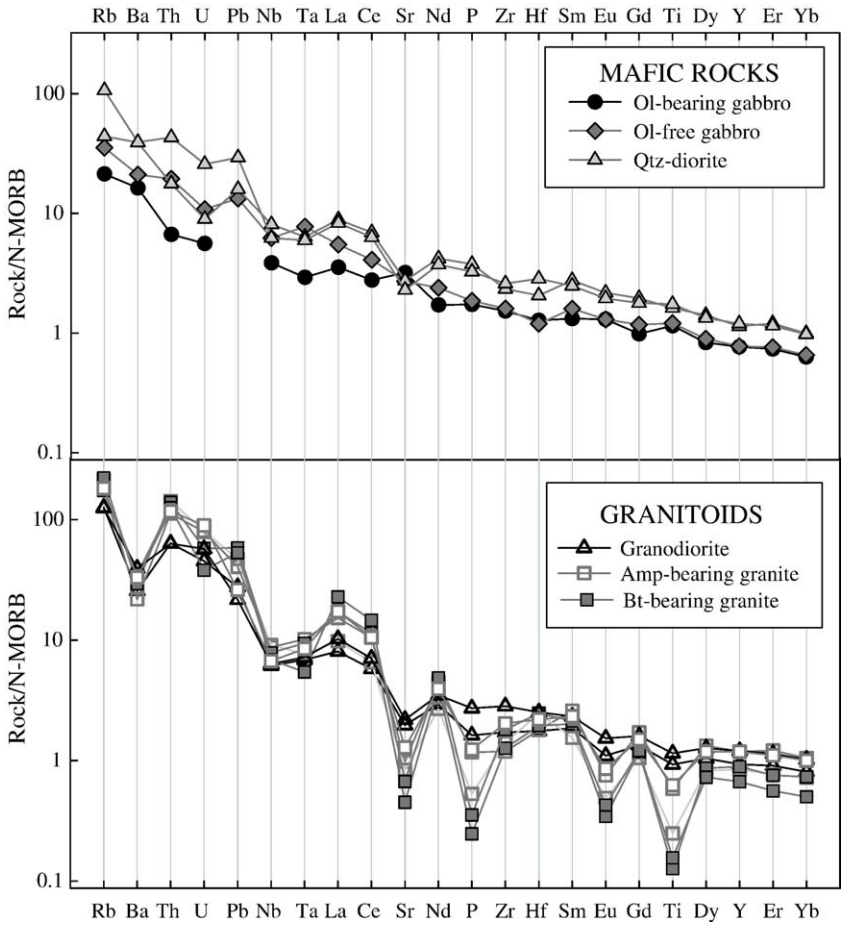

Fig. 5. Whole-rock incompatible trace element compositions, normalised to N-MORB (Hofmann, 1988).

(Poitrasson et al., 1995) were collected from the same area and yield $\varepsilon_{Nd(280\,Ma)}$ of +4.5 and +0.8, respectively, thus showing that mafic rocks are markedly isotopically heterogeneous at least at the metre-scale (Table 5).

3.2. Granitoids

The granitoids are metaluminous to slightly peraluminous, with molar $Al_2O_3/(CaO+Na_2O+K_2O)$ ratios

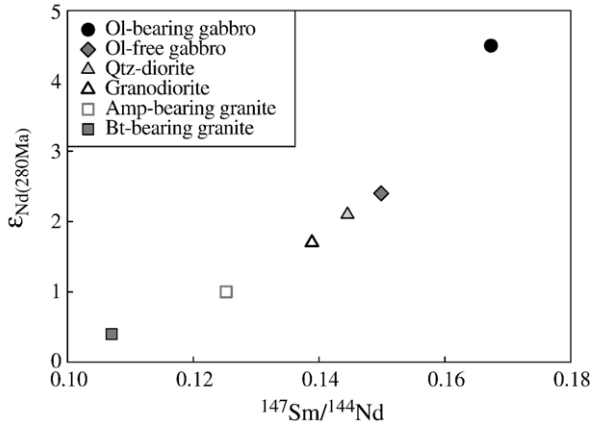

Fig. 6. Plot of ε_{Nd} calculated at 280 Ma vs. $^{147}Sm/^{144}Nd$.

Table 5
Nd isotope compositions of selected samples

Sample	Rock-type	$^{143}Nd/^{144}Nd \pm 2$ S.E.	$^{147}Sm/^{144}Nd$	$^{143}Nd/^{144}Nd_{(280\,Ma)}$	ε_{Nd}	$\varepsilon_{Nd\ (280\,Ma)}$
PO5/2	Ol-G	0.512813±6	0.167	0.51251	+3.4	+4.5
PO16	Cpx-G	0.512673±4	0.150	0.51240	+0.7	+2.4
PO12/1	Qtz-D	0.512650±3	0.145	0.51239	+0.2	+2.1
PO26/2	Gr	0.512618±7	0.139	0.51236	−0.4	+1.7
PO26/1	Amp-G	0.512559±8	0.125	0.51233	−1.5	+1.0
OT6/1	Bt-G	0.512492±3	0.107	0.51230	−2.8	+0.4

Ol-G, olivine-bearing gabbro; Cpx-G, olivine-free gabbro; Qtz-D, quartz-diorite; Gr, granodiorite; Amp-G, amphibole-bearing granite; Bt-G, biotite-bearing granite. 2 S.E. is the uncertainty on measured $^{143}Nd/^{144}Nd$ (internal precision). $^{147}Sm/^{144}Nd$ calculated on the basis of Sm–Nd data obtained by ICP-MS (see Table 4).

ranging from 0.8 for the granodiorites to 1.1 for the biotite granites. In particular, the SiO_2 content progressively increases from granodiorites to amphibole granites and biotite granites, and is negatively correlated with Mg#, Al_2O_3, CaO and TiO_2 (Fig. 4).

The different granitoid types show similar N-MORB-normalised trace element patterns, which are characterised by a marked enrichment of highly incompatible elements (Rb, Ba, Th, U and Pb) over HFSE and REE (Fig. 5). In particular, the Rb and Th provide the highest normalised values. Sr, P, Eu and Ti record a marked decrease from granodiorites to amphibole granites and biotite granites. Conversely, Rb, Th, Pb and LREE increase slightly. In addition, the biotite granites differ from the other granitoids in the lowest HREE concentrations.

The biotite granite selected for the Nd isotope analysis shows the lowest initial ε_{Nd} (+0.4; Fig. 6). This value falls within the range determined by Poitrasson et al. (1995) for the Ota "white" granites (from −0.3 to +0.6). Granodiorite PO26-2 and amphibole granite PO26-1, collected from the same rock body, have initial ε_{Nd} at +1.7 and +1.0, respectively.

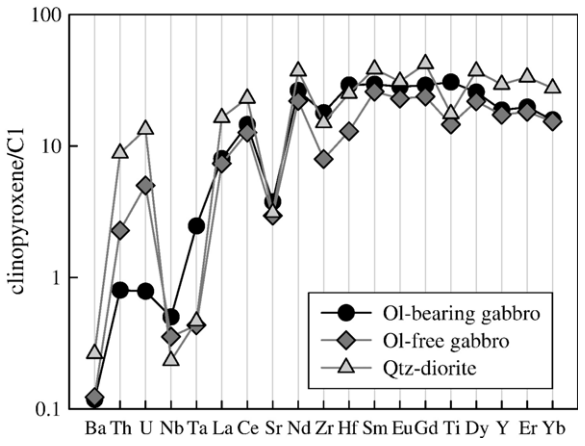

Fig. 7. Incompatible trace element compositions of clinopyroxenes, normalised to C1 chondrite (Anders and Ebihara, 1982).

4. Trace element mineral compositions

4.1. Clinopyroxene

The chondrite-normalised incompatible elements pattern of clinopyroxene from the olivine gabbro is

Table 6
Trace element clinopyroxene compositions (ppm, average values and standard deviation) obtained with LA-ICP-MS

Sample	PO5/2		PO16		PO12/1	
Rock-type	Ol-G		Cpx-G		Qtz-D	
No. of analyses	6	1σ	7	1σ	1	1σ
V	595	15	451	27	428	–
Cr	1840	434	1402	308	6.7	–
Sc	194	17	132	7	134	–
Ti	13,350	537	6,353	574	7,660	–
Sr	29.4	1.2	23.0	1.5	24.3	–
Ba	0.28	0.05	0.29	0.13	0.62	–
Zr	70.6	6.3	31.4	3.5	59.1	–
Nb	0.12	0.02	0.09	0.02	0.06	–
Y	29.3	0.9	26.9	2.4	45.9	–
Hf	3.02	0.29	1.35	0.30	2.62	–
Ta	0.04	0.01	0.01	0.00	0.01	–
Th	0.02	0.01	0.07	0.04	0.26	–
U	0.01	0.01	0.04	0.02	0.11	–
La	1.88	0.07	1.73	0.10	3.85	–
Ce	8.78	0.62	7.64	0.82	13.92	–
Pr	1.86	0.10	1.54	0.19	2.73	–
Nd	11.9	1.0	10.0	0.7	16.8	–
Sm	4.33	0.28	3.81	0.53	5.65	–
Eu	1.58	0.09	1.28	0.16	1.74	–
Gd	5.69	0.31	4.67	0.60	8.30	–
Tb	0.91	0.06	0.84	0.15	1.41	–
Dy	6.24	0.38	5.30	0.89	9.00	–
Ho	1.20	0.05	1.11	0.11	1.76	–
Er	3.14	0.21	2.89	0.39	5.31	–
Tm	0.42	0.02	0.37	0.09	0.70	–
Yb	2.57	0.08	2.50	0.41	4.47	–
Lu	0.38	0.02	0.36	0.09	0.69	–

Ol-G, olivine-bearing gabbro; Cpx-G, olivine-free gabbro; Qtz-D, Quartz-diorite. 1σ = standard deviation of the mean.

characterised by a marked depletion of Ba, Th, U, Nb, Ta and Sr relative to LREE, which are in turn depleted relative to MREE (Fig. 7). There is also a slight enrichment of Th and U relative to Nb and Ba, and a slight depletion of Zr, Hf and HREE relative to MREE. The patterns of the clinopyroxenes from olivine-free gabbro and quartz-diorite differ mainly in the remarkable enrichment of Th and U. The fractionation between Ba, Th, U and LREE is nearly parallel in the clinopyroxenes from olivine-free gabbro and quartz-diorite, with the highest values pertaining to the clinopyroxene from quartz-diorite. The highest contents of Cr, Sc and V have been found for the clinopyroxene from the olivine gabbro (Table 6).

4.2. Amphibole

Red–brown amphibole from the gabbros and quartz-diorites has similar REE compositions (Fig. 8). Its pattern is characterised by slight LREE and HREE depletion relative to MREE, and negative Eu anomaly. The REE pattern of greenish to green amphibole rims is roughly parallel to that of the red–brown cores, but at lower concentration levels. The chondrite-normalised incompatible trace element patterns of red–brown amphibole from the gabbros and quartz-diorites are nearly coincident (Fig. 9). In particular, red–brown amphibole from the olivine gabbro has slightly lower Rb, Ba and Pb, and slightly higher Zr and Hf than that from the olivine-free gabbro and quartz-diorites. In olivine-free gabbro and quartz-diorites, the greenish to green amphibole rims have lower Ba, Nb, Ta, Zr, Hf, Ti, V and Sc than red–brown cores.

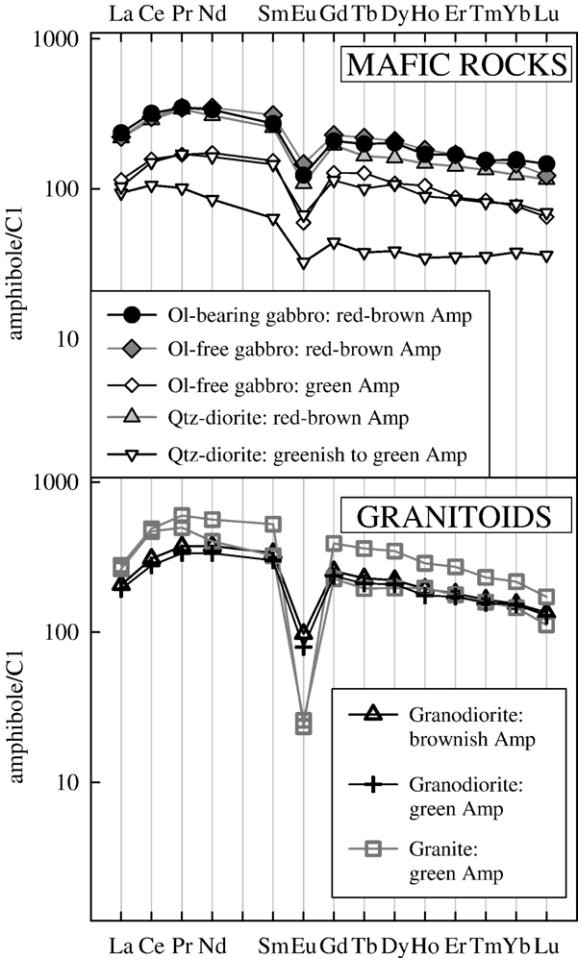

Fig. 8. REE compositions of amphiboles, normalised to C1 chondrite (Anders and Ebihara, 1982).

Although brownish and green amphiboles from granodiorites are characterised by significant variations in major element contents (Table 3), they display homogeneous REE compositions. Their REE patterns are overall similar to those of red–brown amphiboles from mafic rocks, but differ in the steeper negative Eu anomaly. Amphiboles from granites display an abrupt negative Eu anomaly and the highest LREE concentrations (Fig. 8). In granodiorites, the brownish amphibole cores have slightly higher concentrations of Rb, Ba, Sr and Ti and lower Cr contents (Fig. 9; Table 7) than green rims. Amphiboles from granites display the lowest Ba, Sr, Zr and Hf abundances.

5. Discussion

5.1. The evolution of Ota mafic rocks

Mafic rocks show low Mg# ($MgO/MgO+FeO^{tot}$), Cr and Ni values, which decrease from the olivine gabbro to quartz-diorites (Fig. 4; Table 4). In addition, olivine from the least evolved sample is forsterite-poor (62 mol %). These chemical features indicate that the gabbros were derived from melts that had previously undergone an extensive fractional crystallisation. Within mafic rocks, the Mg# decrease from olivine gabbro to quartz-diorite is negatively correlated to Al_2O_3, CaO, TiO_2 and MnO. In particular, the TiO_2 and MnO increase argues against a mixing process between primitive basic and acid melts (presently represented by the gabbros and biotite granites, respectively) for the origin of quartz-diorites. As a whole, major element variations are consistent with a process controlled by fractional crystallisation of plagioclase and clinopyroxene (±olivine). This also agrees with the overall increase of incompatible trace elements from gabbros to quartz-diorites, which results in nearly parallel patterns (Fig. 5). The development of a negative Sr anomaly in the pattern

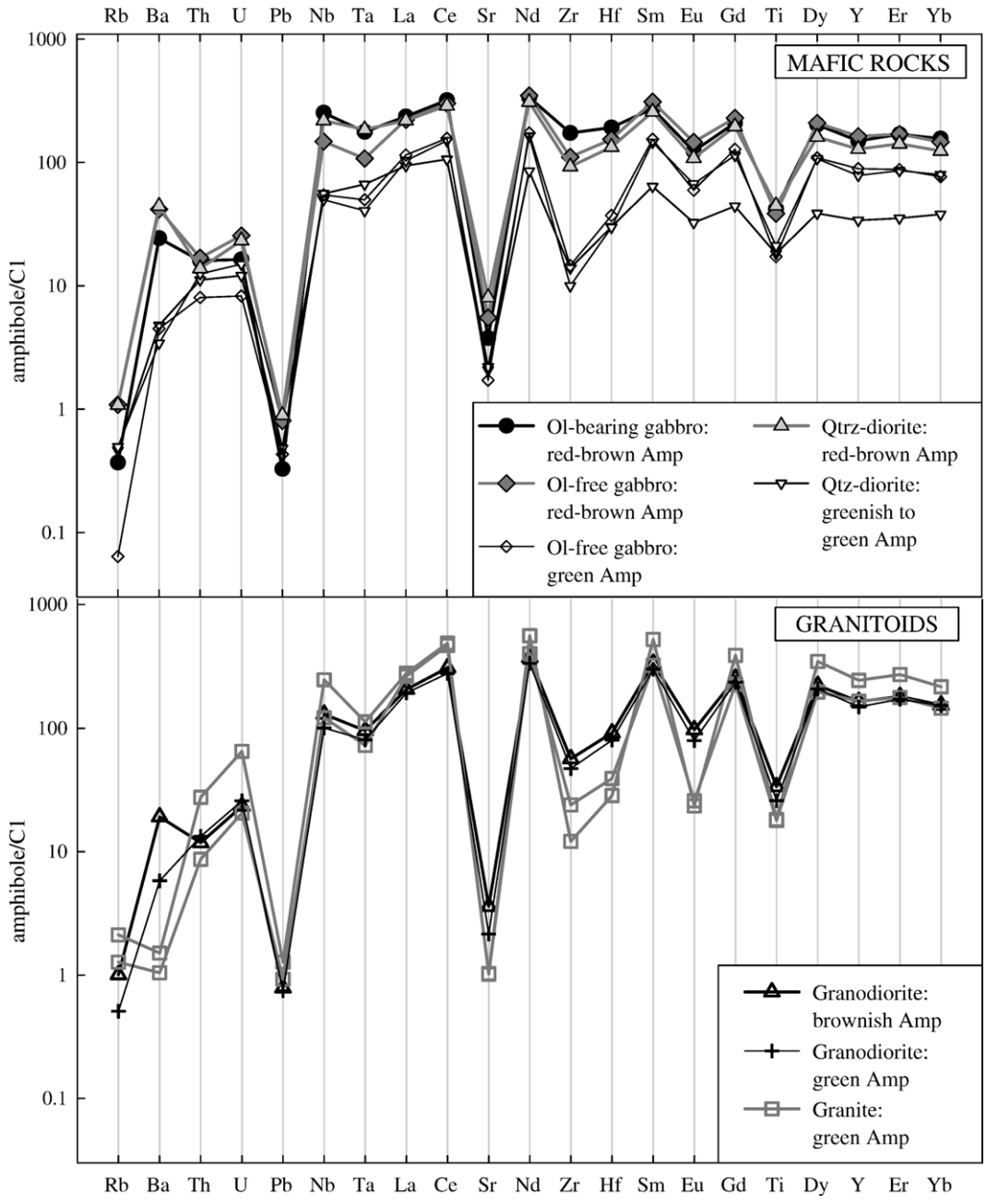

Fig. 9. Incompatible trace elements compositions of amphiboles, normalised to C1 chondrite (Anders and Ebihara, 1982).

of quartz-diorites is in good accordance with a fractional crystallisation process involving a substantial segregation of plagioclase (e.g. Tribuzio et al., 1999a), for which this element is compatible.

The decrease of initial ε_{Nd} from olivine gabbro to olivine-free gabbro and quartz-diorite, and the enrichment in Rb, Th, U and Pb are, however, not consistent with a process of simple fractional crystallisation controlled by plagioclase and clinopyroxene (±olivine). The whole-rock Th and U variations are also paralleled by mineral composition. Remarkably, clinopyroxenes from olivine-free gabbro and quartz-diorite PO12/1 are enriched in Th and U relative to that from the olivine gabbro (Fig. 7). This indicates that the Th and U variations observed for the whole-rocks are not related to a low temperature alteration, such as the one that led to the local alteration of plagioclase. As a whole, the variations of ε_{Nd}, Rb, Th, U and Pb are thus attributed to

Table 7
Trace element amphibole compositions (ppm, average values and standard deviation) from selected samples obtained with LA-ICP-MS

Sample	PO5/2		PO16		PO16		PO23		PO23		PO12/1		PO26/2		PO26/2		PO26-1		PO21	
Rock-type	Ol-G		Cpx-G		Cpx-G		Qtz-D		Qtz-D		Qtz-D		Gr		Gr		Amp-G		Amp-G	
Amp	Red–brown core		Red–brown core		Green rim		Red–brown core		Greenish to green rim		Greenish to green rim		Brownish core		Green rim		Core		Core	
No. of analyses	2	1σ	7	1σ	1	1σ	2	1σ	6	1σ	4	1σ	2	1σ	2	1σ	2	1σ	2	1σ
V	217	70	483	121	383	–	512	34	219	43	388	93	458	45	505	31	153	20	324	107
Cr	3.32	1.34	10.2	8.2	34.8	–	92.3	35.7	31.5	11.2	5.94	1.59	9.80	1.84	186	64	7.74	2.54	31.7	26.9
Sc	54.0	4.3	111.2	19.4	49.0	–	130.9	1.4	45.3	13.8	92.5	26.0	166	7	120	13	148	29	92.1	13.8
Ti	18,348	337	16,770	1,628	7,507	–	19,513	2,804	7,945	889	9,193	178	14,690	1,081	11,313	247	7,971	339	7,788	992
Rb	0.85	0.18	2.50	0.20	0.15	–	2.49	0.32	1.07	0.24	1.14	0.14	2.31	0.39	1.17	0.22	4.87	1.19	2.92	0.45
Sr	29.4	3.7	43.1	12.3	13.4	–	62.8	17.2	16.3	3.5	17.2	2.2	28.1	5.3	16.8	0.7	8.02	0.11	7.94	0.93
Ba	57.0	19.4	97.6	18.6	10.5	–	104	22	11.2	2.4	8.00	1.16	44.8	14.4	13.6	1.4	3.53	0.61	2.44	1.06
Zr	684	3	436	63	57.7	–	364	53	54.8	7.3	39.3	5.0	223	2	186	30	47.8	0.9	94.4	4.6
Nb	62.2	14.4	36.4	3.5	13.4	–	53.9	0.8	13.8	2.5	12.3	1.6	32.0	3.4	24.7	2.4	61.0	2.5	30.1	3.3
Y	233	25	254	33	139	–	200	34	52.9	6.1	122	14	257	2	233	52	382	37	259	18
Hf	20.0	0.0	16.0	2.6	3.87	–	13.9	2.1	3.13	0.42	3.09	0.28	9.55	0.19	8.36	1.43	2.97	0.50	4.08	0.12
Ta	2.52	0.50	1.53	0.12	0.71	–	2.63	0.50	0.94	0.19	0.58	0.06	1.36	0.04	1.15	0.07	1.60	0.02	1.03	0.08
Pb	0.81	0.22	1.99	1.18	1.06	–	2.20	0.09	1.19	0.17	1.90	0.19	1.94	0.09	1.84	0.04	3.14	0.53	2.28	0.59
Th	0.47	0.18	0.50	0.28	0.24	–	0.41	0.06	0.33	0.04	0.37	0.07	0.35	0.05	0.39	0.06	0.81	0.47	0.26	0.10
U	0.13	0.06	0.21	0.16	0.07	–	0.19	0.02	0.10	0.02	0.12	0.04	0.19	0.08	0.21	0.05	0.53	0.39	0.17	0.07
La	55.4	6.1	52.1	3.7	27.0	–	51.5	8.6	22.1	2.9	24.2	3.0	48.5	5.5	45.5	8.9	65.5	11.2	62.0	2.5
Ce	193	30	181	12	94.8	–	174	30	64.0	8.9	90.8	11.8	187	17	168	29	295	50	283	3
Pr	31.1	1.8	31.0	2.5	15.1	–	30.2	0.9	9.03	1.27	15.3	1.8	33.3	2.5	30.0	5.1	53.4	1.9	44.4	3.6
Nd	152	1	158	19	78.5	–	140	17	38.5	5.4	74.1	10.1	170	10	152	28	255	9	183	15
Sm	40.2	0.1	45.7	6.5	22.7	–	37.8	5.2	9.41	1.14	21.4	3.7	49.5	4.3	44.3	9.5	77.2	8.6	47.7	4.7
Eu	6.90	0.97	8.20	0.89	3.34	–	6.07	1.25	1.82	0.14	3.76	0.52	5.46	0.08	4.46	0.70	1.32	0.20	1.45	0.08
Gd	41.1	1.9	45.1	6.7	25.2	–	38.5	6.0	8.70	1.47	22.4	3.8	50.2	2.1	46.5	12.7	76.8	12.8	44.7	3.8
Tb	7.24	0.54	7.98	1.35	4.63	–	6.01	0.96	1.37	0.25	3.66	0.62	8.32	0.62	7.66	1.46	13.12	2.47	7.1	0.7
Dy	49.2	2.7	50.7	7.9	26.4	–	39.0	6.7	9.39	1.52	26.1	4.7	54.0	3.2	50.7	9.6	84.4	15.6	47.8	4.0
Ho	9.44	0.99	10.1	1.4	5.85	–	8.22	1.16	1.93	0.27	4.98	0.80	10.8	0.1	9.76	1.65	16.0	1.8	11.0	1.0
Er	26.9	4.1	27.0	3.8	13.9	–	22.5	3.0	5.62	0.67	13.6	1.9	28.8	0.9	27.4	4.4	43.4	5.9	28.2	1.6
Tm	3.76	0.57	3.66	0.52	2.03	–	3.24	0.49	0.86	0.11	1.97	0.21	3.98	0.27	3.79	0.90	5.62	0.79	3.85	0.24
Yb	25.4	4.0	23.9	1.4	12.5	–	20.1	2.8	6.17	0.65	12.9	1.7	25.1	0.6	24.8	4.1	35.3	4.1	23.7	0.1
Lu	3.57	0.71	2.99	0.38	1.58	–	2.81	0.20	0.88	0.09	1.69	0.19	3.28	0.02	3.14	0.52	4.18	0.79	2.72	0.15

Ol-G, olivine-bearing gabbro; Cpx-G, olivine-free gabbro; Qtz-D, Quartz-diorite; Gr, granodiorite; Amp-G, amphibole-bearing granite; Bt-G, biotite-bearing granite. 1σ = standard deviation of the mean.

a process of basic magma contamination by crustal material.

The crustal contamination most likely occurred in relation to the interaction with the acid magma that gave rise to the associated biotite granites. This is indicated by the local occurrence of K-feldspar-rich dykelets and veins within the mafic rock bodies, which attest that the evolved melts from the acid magma penetrated the basic mass when it was partially solidified. Contamination by the acid magma is also consistent with the low initial ε_{Nd} value and the high amounts of Rb, Th, U and Pb of biotite granites. A similar process was proposed for the origin of microgranular mafic enclaves within calc-alkaline granitoids from the Corsica–Sardinia batholith (Poli and Tommasini, 1991). Assimilation of acid magma material would be promoted by the heat released by the basic magma along the boundaries between the two magmas, and favoured by relatively low viscosity of the acid magma (see also Poli et al., 1996).

5.2. Origin of amphiboles from mafic rocks

Red–brown amphibole from the Ota gabbros is a late-stage phase, which commonly rims clinopyroxene and invariably shows anhedral shape. In these rocks, the ratios of incompatible element abundances in red–brown amphibole to clinopyroxene (Fig. 10) show significant differences relative to partition coefficients from coexisting amphibole and clinopyroxene pairs in gabbroic assemblages (Tribuzio et al., 1999a,b; Hermann et al., 2001; Tiepolo et al., 2002). With the exception of Sr and Ti, calculated incompatible element ratios for the gabbros of the present study are displaced towards higher values (up to one order of magnitude) than those expected at equilibrium. The high concentrations of incompatible elements in red–brown amphibole may be attributed to a process of melt entrapment, associated with crystallisation of plagioclase, ilmenite and, most likely, clinopyroxene (see also Tribuzio et al., 1999a). The development of plagioclase from an interstitial melt is consistent with the anorthite-depleted compositions of plagioclase rims, and the negative Sr and Eu anomalies in the patterns of red–brown amphibole to clinopyroxene concentration ratios. The segregation of ilmenite is indicated by the fact that it commonly occurs as inclusion within red–brown amphibole, and is consistent with the negative Ti anomaly in the patterns of red–brown amphibole to clinopyroxene concentration ratios.

The ratios of Th and U abundances in red–brown amphibole to clinopyroxene are higher in the olivine gabbro than in olivine-free gabbro. In addition,

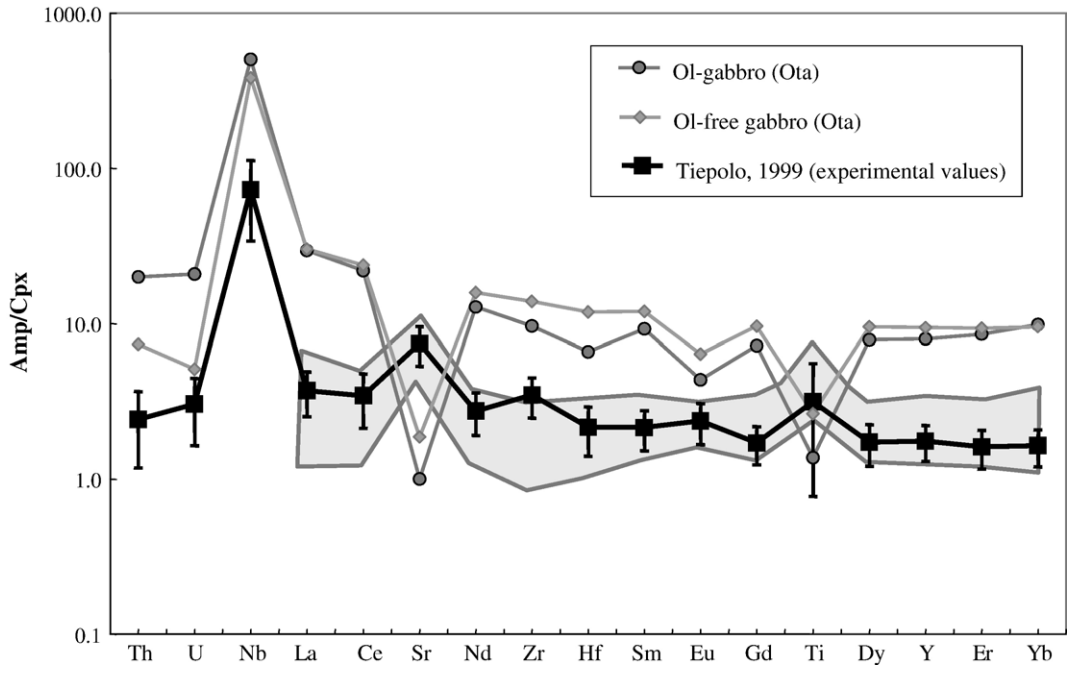

Fig. 10. Red–brown amphibole/clinopyroxene partition ratios for incompatible elements relative to Ota gabbros. Grey field shows the range of partition coefficients between coexisting amphibole and clinopyroxene from gabbroic assemblages (Tribuzio et al., 1999a,b; Hermann et al., 2001; Tiepolo et al., 2002). A dataset of experimental determined $D^{amphibole/clinopyroxene}$ for basaltic system (error bars are 2σ) is also reported for comparative purposes (Tiepolo, 1999).

incompatible element compositions of red–brown amphibole are broadly similar in olivine gabbro, olivine-free gabbro and quartz-diorites (Fig. 9) thus contrasting with the major, trace element and Nd isotope variations observed in the whole rock and in clinopyroxene. We propose that red–brown amphibole from the olivine gabbro formed by percolation within the gabbroic crystal mush of a melt contaminated by the acid magma. The effects of this contamination event are not or partly recorded by incompatible element compositions of clinopyroxene. Remarkably, the relatively low concentrations of Sr, Eu and Ti in red–brown amphibole from mafic rocks could be not only related to the process of melt entrapment, but be enhanced by the high crustal component of the percolating melt, as suggested by the low concentrations of these elements in biotite granites.

The greenish to green amphibole rims have lower REE, Ba, Nb, Ta, Zr, Hf, Ti, V and Sc than red–brown cores. The overall decrease of incompatible elements of amphibole rims relative to the red–brown cores (Fig. 9) could be related to a late stage of the process of trapped melt crystallisation, in response to the formation of red–brown amphibole, ilmenite, apatite, zircon and biotite. The observed depletion of incompatible elements can be accounted for by segregation of this mineral assemblage from a chemically evolved, silicic melt (see also Gillis and Meyer, 2001). However, the local occurrence of oscillatory zoning within the amphibole rims in quartz-diorite contrasts with a process of trapped melt crystallisation. Remarkably, the amphibole rims are also geochemically distinct from green amphibole from contact granitoids. In particular, the greenish to green amphibole rimming red–brown cores in mafic rocks has lower total REE and Y contents, and a less marked negative Eu anomaly than amphibole from contact granitoids (Fig. 8). The formation of greenish to green amphibole in mafic rocks was therefore not directly related to the hybridisation process that promoted the development of amphibole-bearing granitoids (see following sections). We conclude that the late amphiboles within the Ota mafic rocks formed by interaction of the red–brown amphibole grains with late-magmatic aqueous fluids. This hypothesis is sustained by experimental results indicating that most trace elements have low compatibility for aqueous fluids (e.g. Adam et al., 1997).

5.3. The petrogenetic affinity of Ota basic melts

The most primitive sample of the Ota mafic sequence (the olivine gabbro) most likely registers the contamination by the acid magma that gave rise to associated biotite granites, as indicated by the trace element composition of red–brown amphibole (see preceding section). In addition, we cannot unravel whether the earlier fractional crystallisation history was associated with another crustal contamination event, thus precluding an accurate determination of primary melt compositions. Nevertheless, it is noteworthy that the rather high initial ε_{Nd} (+4.5) of the olivine gabbro implies an extensive contribution from a depleted mantle source for the parental basic melts of Ota. The moderate enrichment of LILE, Nb, Ta and LREE in the whole-rock, clinopyroxene and amphibole also rule out a formation by alkaline plume-type melts. In particular, clinopyroxene and amphiboles in rocks derived from plume-type melts differ from those of Ota mafic rocks in the more marked LILE, Nb, Ta and LREE enrichments (e.g. Zanetti et al., 1995). Furthermore, the composition of plagioclase (An = 65–42 mol%, Renna, 2004) associated with olivine in the Ota sample contrasts with the anorthite-rich composition of plagioclase (An > 82 mol %) from arc-related cumulates (Beard, 1986), thus arguing against an origin from subduction-related melts. This notion is consistent with the fact that the evolved mafic rocks from the mafic sequence (i.e. the quartz-diorites) point to a decrease of Mg# associated with an increase of TiO_2 and MnO relative to gabbros, thus arguing against typical calc-alkaline differentiation trends.

Other gabbroic sequences from the Corsica batholith are geochronologically and geochemically similar to the Ota mafic body (Paquette et al., 2003; Cocherie et al., 2005). For instance, the least contaminated samples of coeval Pila Canale and S. Lucia mafic complexes have initial ε_{Nd} value of +4.3 (Cocherie et al., 1994) and +5.5 (Paquette et al., 2003), respectively. The Ota olivine gabbro is also geochemically similar to the olivine gabbros of post-Variscan mafic complex of Sondalo (Central Alps), which have initial ε_{Nd} ranging from +2.8 to +4.4 (Tribuzio et al., 1999b). In particular, clinopyroxene and amphibole from Ota and Sondalo olivine-bearing rocks have nearly coincident incompatible element fingerprint. The involvement of a crustal contribution in the petrogenesis of Sondalo olivine gabbros was recognised on the basis of their somewhat elevated $\delta^{18}O_{Cpx}$ (Tribuzio et al., 1999b).

In the Alpine belt, evidence for parental melts derived from typical depleted mantle sources are preserved in some of the post-Variscan gabbroic complexes (e.g. initial ε_{Nd} up to +8.5; Voshage et al., 1990; Thöni and Jagoutz, 1992; Hermann et al., 2001;

Montanini and Tribuzio, 2001). Commonly, the MORB-type affinity of parental melts was recognised after having ruled out the role of crustal contamination, which was associated with their emplacement at lower crustal levels. The involvement of depleted mantle sources was attributed to a geodynamic process of lithospheric extension, in response to post-thickening gravitational collapse of the Variscan orogeny (see also Costa and Rey, 1995; Müntener et al., 2000). This event was most likely correlated with the diffuse mafic intrusions that affected the Corsica–Sardinia batholith at about 280 Ma.

5.4. Amphibole-bearing granitoids: evidence for magma hybridisation

The amphibole-bearing granodiorites to granites are found along the contacts between mafic rocks and biotite granites, and contain mafic enclaves and glomeroporphyritic clots rich in amphibole and biotite (see also Platevoet and Bonin, 1991). These textures indicate that the basic magma was disrupted into the acid magma, thus leading to the formation of hybrid amphibole-bearing granitoids. The quartz ocelli rimmed by amphibole coronas in the amphibole-bearing granitoids represent another textural evidence for magma hybridisation (Sato, 1975; Hibbard, 1991; Vernon, 1991). Most likely, these quartz grains nucleated in the acid melt, did not completely dissolve when they came in contact with the liquid phase of the basic magma and promoted the nucleation of fine-grained amphibole on their rims. The development of quartz crystals within the acid magma probably resulted in high viscosity conditions (Thompson and Dungan, 1985; Sparks and Marshall, 1986; Poli et al., 1996), which prevented thorough homogenisation with the basic magma and inhibited the development of a large volume of amphibole-bearing granitoids.

The amphibole-bearing granitoids of the Ota association have major element and Nd isotope compositions that lie between a basic end-member similar to the mafic rocks and an acid end-member similar to biotite granites (Figs. 4 and 6). These chemical covariations do not imply a homogeneous mixing between two silicate melts with different compositions, which would contrast with the mingling textural relations, but confirm that the amphibole-bearing granitoids formed through a process of hybridisation between basic and acid magmas. In particular, the presence of K-feldspar rich dykelets in the contact zone shows the segregation of K-rich residual melts, which in turn imply the occurrence of processes of mineral fractionation and accumulation. Remarkably, some of the trace element concentrations of amphibole-bearing granitoids (e.g. U and Y) plot away from a mixing line between basic and acid components, as already shown by Platevoet and Bonin (1991). The decoupling between major and trace elements can be attributed to the late fractionation processes, as already shown in other gabbro–granite hybrid terrains (e.g. Bedard, 1990; Tate et al., 1997).

To unravel the extent of hybridisation of the selected amphibole-bearing granitoids, we have carried out two-component calculations based on Nd isotope compositions, which should not be affected by late fractionation processes. In particular, we have reproduced the initial ε_{Nd} of hybrid granitoids PO26-2 and PO26-1 assuming the initial ε_{Nd} of biotite granite OT6/1 as representative of the acid component. The whole range of initial ε_{Nd} of Ota mafic rocks has been imposed as the basic component, because the basic melt could be variably evolved through fractional crystallisation and concomitant assimilation of acid magma before the "contact" hybridisation process. The Nd isotope composition of granodiorite PO26-2 and granite PO26-1 imply a fraction of basic component varying from 32% to 75% and 15% to 35%, respectively, thus indicating that the amphibole-bearing granitoids record different basic to acid component ratios.

Further constraints about the hybridisation process recorded by the Ota amphibole-bearing granitoids are given by amphibole compositions. Major and trace element compositions of brownish amphibole cores from contact granodiorites are similar to those of red–brown amphiboles from mafic rocks (Figs. 8 and 9, Table 7). This indicates that brownish amphibole cores from the granodiorites were derived from grains nucleated in the basic magma. The green amphibole rims from granodiorites have lower concentrations of Rb, Ba and Sr, which may result from the equilibration with K-feldspar, and higher Cr amounts than the brownish cores (ca. 190 and 10 ppm, respectively). The Cr enrichment can be attributed to dissolution of clinopyroxene grains from the basic magma, in agreement with the high Cr amounts (1840 to 1400 ppm) observed for the clinopyroxenes from the Ota gabbros. Probably, the process of chemical reaction of the clinopyroxene grains with the acid melt promoted the amphibole overgrowth and enabled the preservation of the trace element signature of pristine amphibole grains nucleated in the basic magma, i.e. prevented the equilibration of the brownish cores with the acid magma.

Amphibole from contact granites is chemically homogeneous and distinct from the amphibole grains within the mafic rocks. Remarkably, the slight LREE enrichment of amphiboles from granites relative to

amphiboles from granodiorites most likely reflects the higher proportion of acid component involved in the origin of the amphibole granites, in agreement with the more marked LREE enrichment of biotite granites relative to mafic rocks (Fig. 5). The amphibole growth in contact granites could be related to a process of compositional gradient-induced diffusion from the basic to the acid melt. Such a process presumably favoured the introduction of Ca, Mg, Fe and Al into the acid host and thus promoted the crystallisation of amphibole. This hypothesis is supported by the experimental studies of Watson and Jurewicz (1984) that indicate that a spatially limited chemical diffusion of Ca, Mg, Fe and Al from the basic to the acid melt may occur under plutonic conditions (see also Eberz and Nicholls, 1990; Orsini et al., 1991). We thus propose that the development of amphibole in contact granitoids is related not only to the occurrence of mafic minerals in the basic magma, but also to chemical diffusion processes.

6. Conclusions

The gabbro–granite association of Ota (Corsica–Sardinia batholith) developed during the latest stages of the Variscan cycle, as a result of the interaction between basic melts derived from a depleted mantle source and metaluminous to slightly peraluminous acid magmas. The intrusion of these mantle-derived melts has been related to a batholith-scale magmatic episode that occurred at about 280 Ma, in response to lithospheric extension subsequent to the Variscan collision.

The Ota basic melts evolved through fractional crystallisation and concomitant assimilation of the acid magma. The contamination of the basic melt is notably registered by the variations of Th and U concentrations in clinopyroxene from mafic rocks. Remarkably, the incompatible element compositions of anhedral amphibole from the most primitive mafic rocks, which lack textural evidence for magma hybridisation, show that the whole Ota mafic sequence was affected by the acid magma contamination.

Hybridisation between basic and acid magmas is also shown by the limited development of amphibole-bearing granodiorites to granites along the contacts between the mafic rock bodies and enclosing biotite granites. In particular, amphibole from contact granodiorites displays major and trace element zonings, which document reactions between crystals from the basic magma (amphibole and clinopyroxene) and acid melt. Conversely, amphibole from contact granites is chemically homogeneous, thus suggesting that such a late hybridisation process comprised also a process of gradient-induced chemical diffusion.

Acknowledgements

We thank F. Bussy for thorough and constructive review of an earlier version of the manuscript. Two anonymous reviewers provided useful comments to the submitted manuscript. This work was financially supported by Ministero dell'Università e della Ricerca Scientifica (Progetti di Ricerca di Interesse Nazionale), Università di Pavia (Fondi di Ateneo per la Ricerca) and Consiglio Nazionale delle Ricerche (C.N.R.).

References

Adam, J., Green, T.H., Sie, S.H., Ryan, C.G., 1997. Trace element partitioning between aqueous fluids, silicate melts and minerals. Eur. J. Mineral. 9, 569–584.

Anders, E., Ebihara, M., 1982. Solar system abundances of the elements. Geochim. Cosmochim. Acta 46, 2363–2380.

Beard, J.S., 1986. Characteristic mineralogy of arc-related cumulate gabbros: implications for the tectonic setting of gabbroic plutons and for andesite genesis. Geology 14 (10), 848–851.

Bedard, J., 1990. Enclaves from A-type granite of the Mégantic Complex, White Mountain Magma Series; clues to granite magmagenesis. J. Geophys. Res. 95, 17797–17819.

Blundy, J.D., Shimizu, N., 1991. Trace element evidence for plagioclase recycling in calc-alkaline magmas. Earth Planet. Sci. Lett. 102, 178–197.

Bonin, B., 1988. Peralkaline granites of Corsica: some petrological and geochemical constraints. Rend. Soc. Ital. Mineral. Petrol. 43, 281–306.

Bonin, B., 2004. Do coeval mafic and felsic magmas in post-collisional to within-plate regimes necessarily imply two contrasting, mantle and crustal, sources? A review. Lithos 78, 1–24.

Bonin, B., Grelou-Orsini, C., Vialette, Y., 1978. Age, origin and evolution of the anorogenic complex of Evisa (Corsica): K–Li–Rb–Sr study. Contrib. Mineral. Petrol. 65, 425–432.

Bonin, B., Azzouni-Sekkal, A., Bussy, F., Ferrag, S., 1998. Alkali-calcic and alkaline post-orogenic (PO) granite magmatism: petrologic constraints and geodynamic settings. Lithos 45, 45–70.

Cocherie, A., Rossi, P., Fouillac, A.M., Vidal, P., 1994. Crust and mantle contributions to granite genesis—an example from the Variscan batholith of Corsica, France, studied by trace element and Nd–Sr–O isotope systematics. Chem. Geol. 115, 173–211.

Cocherie, A., Rossi, Ph., Fanning, C.M., Guerrot, C., 2005. Comparative use of TIMS and SHRIMP for U–Pb zircon dating and mafic tholeiitic layered complexes and dykes from the Corsican Batholith (France). Lithos 82, 185–219.

Costa, S., Rey, P., 1995. Lower crustal rejuvenation and growth during post thickening collapse: insights from a crustal cross section through a Variscan metamorphic core complex. Geology 23, 905–908.

Eberz, G.R., Nicholls, I.A., 1990. Chemical modification of enclave magma by post-emplacement crystal fractionation, diffusion and metasomatism. Contrib. Mineral. Petrol. 104, 47–55.

Edel, J.B., Montigny, R., Thuizat, R., 1981. Late Paleozoic rotations of Corsica and Sardinia: new evidence from paleomagnetic and K–Ar studies. Tectonophysics 79, 201–223.

Egeberg, A.T., Bonin, B., Sorensen, H., 1993. The Bonifatto peralkaline granites (NW Corsica): a possible case of evolution through volatile transfer. Bull. Soc. Géol. Fr. 164 (5), 739–758.

Ferré, E.C., Leake, B., 2001. Geodynamic significance of early orogenic high-K crustal and mantle melts: example of the Corsica batholith. Lithos 59, 47–67.

Gillis, K.M., Meyer, P.S., 2001. Metasomatism of oceanic gabbros by late stage melts and hydrothermal fluids: evidence from the rare earth element composition of amphiboles. Geochem. Geophys. Geosyst. 2 (Paper number 2000GC000087).

Hermann, J., Müntener, O., Günther, D., 2001. Differentiation of mafic magma in a continental crust-to-mantle transition zone. J. Petrol. 42, 189–206.

Hibbard, M.J., 1991. Textural anatomy of twelve magma-mixed granitoid systems. In: Didier, J., Barbarin, B. (Eds.), Enclaves and Granite Petrology. Developments in Petrology, vol. 13. Elsevier, Amsterdam, pp. 431–444.

Hofmann, A.W., 1988. Chemical differentiation of the Earth: the relationship between mantle, continental crust, and oceanic crust. Earth Planet. Sci. Lett. 90, 297–314.

Kretz, R., 1983. Symbols for rock-forming minerals. Am. Mineral. 68, 277–279.

Leake, B.E., Woolley, A.R., Arps, C.E.S., Birch, W.D., Gilbert, M.C., Grice, J.D., Hawthorne, F.C., Kato, A., Kisch, H.J., Krivovichev, V.G., Linthout, K., Laird, J., Mandarino, J., Maresch, W.V., Nickel, E.H., Tock, N.M.S., Schumacher, J.C., Smith, D.C., Stephenson, N.C.N., Ungaretti, L., Whittaker, E.J.W., Youzhi, G., 1997. Nomenclature of amphiboles: report of the Subcommittee on amphiboles of the International Mineralogical Association Commission on new minerals and mineral names. Am. Mineral. 82, 1019–1037.

Montanini, A., Tribuzio, R., 2001. Gabbro-derived granulites from the Northern Apennines (Italy): evidence for lower-crustal emplacement of tholeiitic liquids in post-Variscan times. J. Petrol. 42, 2259–2277.

Müntener, O., Hermann, J., Trommsdorff, V., 2000. Cooling history and exhumation of lower-crustal granulite and upper mantle (Malenco, Eastern Central Alps). J. Petrol. 41, 175–200.

Orsini, J.B., Cocirta, C., Zorpi, M.J., 1991. Genesis of mafic microgranular enclaves through differentiation of basic magmas, mingling and chemical exchanges with their host granitoid magmas. In: Didier, J., Barbarin, B. (Eds.), Enclaves and Granite Petrology. . Developments in Petrology, vol. 13. Elsevier, Amsterdam, pp. 445–464.

Paquette, J.L., Ménot, R.P., Pin, C., Orsini, J.B., 2003. Episodic and short-lived granitic pulses in a post-collisional setting: evidence from precise U–Pb zircon dating through a crustal cross-section in Corsica. Chem. Geol. 198, 1–20.

Platevoet, B., Bonin, B., 1991. Enclaves and mafic–felsic associations in the Permian alkaline province of Corsica, France: physical and chemical interactions between coeval magmas. In: Didier, J., Barbarin, B. (Eds.), Enclaves and Granite Petrology. Developments in Petrology, vol. 13. Elsevier, Amsterdam, pp. 191–204.

Platevoet, B., Bonin, B., Pupin, J.P., Gandolo, A., 1988. Les associations acide–basique du magmatisme alcalin anorogénique de Corse. Bull. Soc. Géol. Fr. 8, 43–55.

Poitrasson, F., Pin, C., Duthou, J.L., Platevoet, B., 1994. Aluminous subsolvus anorogenic granite genesis in the light of Nd isotopic heterogeneity. Chem. Geol. 112, 199–219.

Poitrasson, F., Duthou, J.L., Pin, C., 1995. The relationship between petrology and Nd isotopes as evidence for contrasting anorogenic granite genesis: example of the Corsican Province (SE France). J. Petrol. 36, 1251–1274.

Poli, G., Tommasini, S., 1991. A geochemical approach to the evolution of granitic plutons; a case study, the acid intrusions of Punta Falcone (northern Sardinia, Italy). Chem. Geol. 92, 87–105.

Poli, G., Tommasini, S., Halliday, A.N., 1996. Trace element and isotopic exchange during acid–basic magma interaction processes. Trans. R. Soc. Edinb. Earth Sci. 87, 225–232.

Renna, M.R., 2004. Petrologia e geocronologia U–Pb del complesso di Porto (Corsica Nord-Occidentale). PhD Thesis, Università di Pavia.

Sato, H., 1975. Diffusion coronas around quartz xenocrysts in andesite and basalt from Tertiary volcanic region in northeastern Shikoku, Japan. Contrib. Mineral. Petrol. 50, 49–64.

Sparks, R.S.J., Marshall, L.A., 1986. Thermal and mechanical constraints on mixing between mafic and silicic magmas. J. Volcanal. Geothermal. Res. 29, 99–124.

Tate, M.C., Clarke, D.B., Heaman, L.M., 1997. Progressive hybridisation between Late Devonian mafic-intermediate and felsic magmas in the Meguma Zone of Nova Scotia, Canada. Contrib. Mineral. Petrol. 126, 401–415.

Thompson, R.A., Dungan, M.A., 1985. The petrology and geochemistry of the Handkerchief Mesa mixed magma complex, San Juan Mountains, Colorado. J. Volcanal. Geothermal. Res. 26, 251–274.

Thöni, M., Jagoutz, E., 1992. Some new aspects of dating eclogites in orogenic belts: Sm–Nd, Rb–Sr, and Pb–Pb isotopic results from the Austroalpine Saualpe and Koralpe type-locality (Carinthia/Styria, southeastern Austria). Geochim. Cosmochim. Acta 56, 347–368.

Tiepolo, 1999. Determinazione sperimentale dei coefficienti di distribuzione solido/liquido in anfiboli di mantello: ruolo del controllo cristallochimico. PhD thesis, Università di Pavia.

Tiepolo, M., Tribuzio, R., Vannucci, R., 2002. The compositions of mantle-derived melts developed during the Alpine continental collision. Contrib. Mineral. Petrol. 144, 1–15.

Tiepolo, M., Bottazzi, P., Palenzona, M., Vannucci, R., 2003. A laser probe coupled with ICP-double-focusing sector-field mass spectrometer for in situ analysis of geological samples and U–Pb dating of zircon. Can. Mineral. 41, 259–272.

Tommasini, S., Poli, G., Halliday, A.N., 1995. The role of sediment subduction and crustal growth in Hercynian plutonism: isotopic and trace element evidence from the Sardinia–Corsica batholith. J. Petrol. 36, 1305–1332.

Tribuzio, R., Tiepolo, M., Vannucci, R., Bottazzi, P., 1999a. Trace element distribution within olivine-bearing gabbros from the Northern Appennine ophiolites (Italy): evidence for post-cumulus crystallization in MOR-type gabbroic rocks. Contrib. Mineral. Petrol. 134, 123–133.

Tribuzio, R., Thirlwall, M.F., Messiga, B., 1999b. Petrology, mineral and isotope geochemistry of the Sondalo gabbroic complex (Central Alps, Northern Italy): implications for the origin of post-Variscan magmatism. Contrib. Mineral. Petrol. 136, 48–62.

Vaggelli, G., Olmi, F., Conticelli, S., 1999. Quantitative electron microprobe analysis of reference silicate mineral and glass samples. Acta Vulcanol. 11, 297–303.

van Achterbergh, E., Ryan, C.G., Griffin, W.L., 1999. Glitter: on-line interactive data reduction for the laser ablation ICP-MS microprobe. In: Proceedings of the 9th Annual V.M., Goldschmidt Conference, Boston, USA.

van Tellingen, H.W, Vorschure, R.H., Andriessen, P.A.M., 1996. Indications for an early Miocene mafic dike swarm in western

Corsica. A combined fission track, isotopic and geochemical investigation. Proc. K. Ned. Akad. Wet. 99 (1–2), 85–104.

Vellutini, P., 1975. Sur la structure du massif du granite rouge de Porto (Corse du Nord-Ouest). C. R. Acad. Sci. Paris, Ser. II 280, 813–815.

Vernon, R.H., 1991. Interpretation of microstructures of microgranitoid enclaves. In: Didier, J., Barbarin, B. (Eds.), Enclaves and Granite Petrology. Developments in Petrology, vol. 13. Elsevier, Amsterdam, pp. 277–291.

Voshage, H., Hofmann, A.W., Mazzucchelli, M., Rivalenti, G., Sinigoi, S., Raczek, I., Demarchi, G., 1990. Isotopic evidence from the Ivrea Zone for a hybrid lower crust formed by magmatic underplating. Nature 347, 731–736.

Watson, E.B., Jurewicz, S.R., 1984. Behaviour of alkalies during diffusive interaction of granitic xenoliths with basaltic magma. J. Geol. 92, 121–131.

Wyllie, P.J., Cox, K.G., Biggar, G.M., 1962. The habit of apatite in synthetic systems and igneous rocks. J. Petrol. 3, 238–243.

Zanetti, A., Vannucci, R., Oberti, R., Dobosi, G., 1995. Trace-element compositions and crystal-chemistry of mantle amphiboles from the Carpatho-Pannonian Region. Acta Vulcanol. 7, 265–276.